UC Santa Barbara

UC Santa Barbara Previously Published Works

Title

Metastable Ni

7

B

3

: A New Paramagnetic Boride from Solution Chemistry, Its Crystal Structure and Magnetic Properties

Permalink

https://escholarship.org/uc/item/1hc3r4kb

Journal

Inorganic Chemistry, 54(22)

ISSN

0020-1669 1520-510X

Authors

Hofmann, Kathrin
Kalyon, Nalan
Kapfenberger, Christine
et al.

Publication Date

2015-11-16

DOI

10.1021/acs.inorgchem.5b01929

Peer reviewed

Metastable Ni$_7$B$_3$ – a new paramagnetic boride from solution chemistry, its crystal structure and magnetic properties

Kathrin Hofmann,[a] Nalan Kalyon,[a] Christine Kapfenberger,[a] Leo Lamontagne,[b] Salman Zarrini,[c] Robert Berger,[c*] Ram Seshadri,[b*] and Barbara Albert[a*]

[a] Eduard-Zintl-Institute of Inorganic and Physical Chemistry, Technische Universität Darmstadt, Alarich-Weiss-Str. 12, 64287 Darmstadt, Germany

[b] Materials Department and Materials Research Laboratory, University of California Santa Barbara, Santa Barbara CA 93106, U.S.A.

[c] Fachbereich Chemie, Philipps-Universität Marburg, Hans-Meerwein-Str. 4, 35032 Marburg, Germany

*corresponding author: albert@ac.chemie.tu-darmstadt.de (B. Albert), Tel. +49-(0)6151-162392, FAX +49-(0)6151-166029

Abstract

We trapped an unknown metastable boride by applying low-temperature solution synthesis. Single-phase nickel boride, Ni_7B_3, was obtained as bulk samples of microcrystalline powders when annealing the amorphous, nanoscale precipitate that is formed in aqueous solution of nickel chloride upon reaction with sodium tetrahydridoborate. Its crystal structure was solved based on a disordered Th_7Fe_3-type model (hexagonal crystal system, space group $P6_3mc$, no. 186, a = 696.836(4) pm, c = 439.402(4) pm), using synchrotron X-ray powder data. Magnetic measurements reveal paramagnetism, which is in accordance with quantum chemical calculations. According to high-temperature X-ray diffraction and differential scanning calorimetry this nickel boride phase has a narrow stability window between 300 °C and 424 °C. It crystallizes at ca. 350 °C, then starts decomposing to form Ni_3B and Ni_2B above 375 °C, and shows an exothermic effect at 424 °C.

Keywords

Introduction

Many borides are known to exhibit exceptional physical properties,[1,2] but their uses are limited due to the complexity of their syntheses and handling. Often they are high-melting and of refractory character; and phases that are thermodynamically stable are obtained at high temperatures. Synthetic routes towards metastable phases are rare but recently have gained a lot of interest, leading to new and unexpected varieties of known and novel compounds. Examples are borides obtained as nanoscale particles at moderate temperatures from solvents [3-7] or from salt melts,[8,9] new compounds like Co_5B_{16} from high-pressure-high temperature routes,[10] and novel mechanochemically-synthesized phases like hexagonal OsB_2,[11-13] a metastable ReB_2-type variant of ultra-incompressible, hard orthorhombic OsB_2.[14] ReB_2 has been reported to be superhard.[15]

The Ni-B system comprises several compounds whose crystal structures have been described in literature: $Ni_{23}B_6$, Ni_3B, Ni_2B, Ni_4B_3 (two modifications), NiB, and Ni-doped □-boron.[16-21] They were characterized as soft ferromagnets (metal-rich nickel borides) or paramagnets (boron-rich nickel borides).[22,23] In some cases it is not clear whether the observed ferromagnetism is actually caused by the nickel boride under investigation, or elemental nickel that may be present as a side phase.

The title compound, Ni_7B_3, is among the metal-rich members of the series and its formation was mentioned in literature, but the phase was not obtained as bulk material or crystallographically characterized before. *Wodnieka* et al. observed a side product with this composition when crystallizing amorphous Ni-B alloys,[24] similar to what was seen when thin films of Ni_3B were made by chemical vapor deposition,[25] or during the crystallization of Ni-B metallic glasses.[26] *Machizaud* et al. investigated an amorphous alloy, $Ni_{66}B_{34}$, and postulated Ni_7B_3 to decompose above 500 °C to form Ni_3B and Ni_2B.[27] Lattice parameters are known from electron diffraction.[25]

We will now describe a new bulk synthesis of single-phase Ni_7B_3 that we found to crystallize with a structure that can be classified as an unknown disordered variant of the Th_7Fe_3-structure type. The structure was solved from powder diffraction data. Ni_7B_3 is the first binary boride of a 3d metal that crystallizes with a structure related to Th_7B_3. Other borides of the – ordered – Th_7Fe_3–type are Ru_7B_3, Rh_7B_3, Re_7B_3, and Tc_7B_3,[28-30] or ternary compounds like for example $M_xRh_{7-x}B_3$ (M = Cr, Mn, Ni; x = 0.39–1).[31]

Materials and methods

Low-temperature powder synthesis. A solution of nickel chloride ($NiCl_2 \cdot 6\ H_2O$, 4.0 mmol) in degassed water (200 mL) was added drop-wise within one minute to solid sodium tetrahydridoborate ($NaBH_4$, 4.0 mmol, r.t.) and stirred for one hour. The black and amorphous precipitate was separated by centrifugation, washed three times with water and acetone, and dried in vacuo for two hours. Afterwards the sample was annealed at 375 °C in vacuo for two hours. All of the procedures took place under purified argon. The product is a very fine crystalline powder.

Structural characterization. Crystalline powders were filled into capillaries and measured at a powder diffractometer with synchrotron radiation at HASYLAB/DESY (Hamburg, Germany, beam line B2, λ = 49.9694 pm, Ge(111) double monochromator, Ge(111) analyzer, NaI scintillation counter). Structure refinements were performed using the Rietveld method, program GSAS.[32] Positional parameters and occupancies were refined freely. Isotropic displacement parameters were refined, too. High-temperature X-ray powder diffraction data were collected by a powder diffractometer (STOE Stadi P, position-sensitive detector) with $CuK_{\alpha 1}$ radiation (Ge(111) monochromator, λ = 1.54060 Å, quartz capillary, Debye-Scherrer geometry). Further information on the data collection and crystal structure may be obtained from ref. 33.

Magnetic measurements. Magnetic susceptibility data was acquired under a 100 Oe ($10^5(4\pi)^{-1}$ Am^{-1}) field while cooling under field, between 350 K and 2 K on a Quantum Design MPMS 5XL SQUID magnetometer.

Computational methods. Density functional theory (DFT)[34] calculations were carried out self-consistently using the projected augmented plane wave method (PAW)[35] and a plane wave basis set as implemented in the Vienna ab-initio Simulation Package (VASP).[36] The generalized gradient approximation (GGA) in the form proposed by Perdew–Burke–Ernzerhof[37] was employed for treating the exchange–correlation potential. The plane-wave basis set was expanded to an energy cut-off of 600 eV.

Convergence criterion in the self-consistent field (SCF) procedure was an absolute change in energy that remained below 10^{-8} eV/cell between two consecutive SCF cycles. The Brillouin–zone integration was performed using the first order of the Methfessel-Paxton method[38] with a smearing width of 0.01 eV on a $13 \times 13 \times 18$ Monkhorst-Pack grid.[39] In energy-minimisations

of the structures with a conjugate gradient approach,[40] all degrees of freedom were allowed to relax until the absolute value of all forces dropped below 0.1 eV nm^{-1} (0.01 eV Å^{-1}).

Thermal analysis. Difference scanning calorimetry was performed heating the samples (34.921 mg) in argon with 10K/min from room temperature to 800 °C (corundum crucible, Netzsch STA 449F3).

Results and discussion

Synthesis and crystal structure. Modifying a precipitation route that has been previously employed to synthesize amorphous nickel-boron catalysts[41] and nanoparticles of Ni_3B[3, 42] we were able to prepare a black, nanostructured (according to scanning electron microscopy, see Supporting Information Fig. S1) and X-ray amorphous precipitate. According to energy-dispersive X-ray spectroscopy its ratio of nickel to boron is 7:3. From those precipitates, microcrystalline powders of Ni_7B_3 were obtained reproducibly upon annealing, with no side phase detected by X-ray diffraction. The powder pattern was indexed in the hexagonal crystal system with a = 697.51 pm and c = 439.63 pm, comparable to earlier observations.[25] The extinction conditions do not contradict the most probable space group $P6_3mc$ (no. 186), which is that of Th_7Fe_3. Initially, a Rietveld refinement of the structure based on synchrotron data was attempted based on the ideal Th_7Fe_3-structure type (one two-fold and two six-fold metal atom sites and one sixfold boron site), but the fit resulted in significant differences of the intensities of observed and calculated reflections, especially for the (201) reflection (2Θ at *ca.* 36 °). Careful examination of the difference electron density maps (Fig. 1) showed excess electron density close to the position of one of the nickel atoms, Ni3. Occupying this additional site, Ni4, causes a disordered structure and a better fit of the experimental diffraction data (Fig. 2). One additional atomic site suitable for boron atoms results.

5
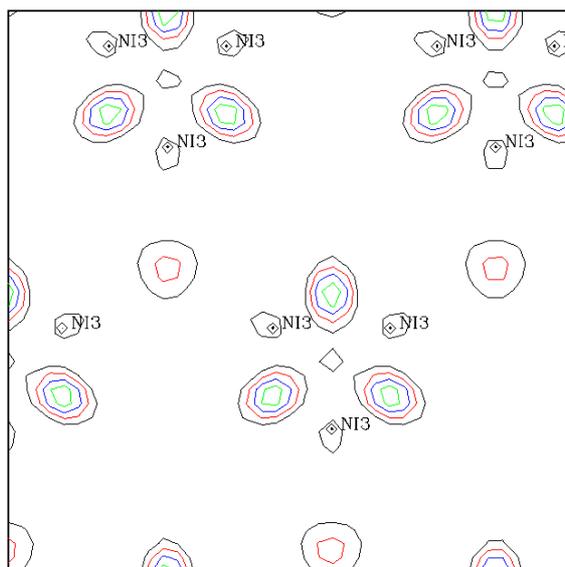
Figure 1. Difference electron density map after fitting the powder data based on the ideal Th_7Fe_3-structure type, indicating residual electron density caused by the structural disorder

The distance between the positions that are partially occupied with Ni3 and Ni4 is of course very short (152.31 pm). Site occupation factors for Ni3 and Ni4 were constrained to a shared value of one and refined together. Boron atoms were positioned inside two voids of the nickel atom structure and their positional parameters were refined freely. The occupation factors for the two boron atom sites were refined freely as well. Table 1 and table 2 summarize the information on data collection, structure refinement, and crystal structure. It should be noted that the displacement parameters of the Ni atoms are better when X-ray powder diffraction data collected with $CuK_{\alpha 1}$ radiation is used (see Supporting Information, Table S2, Figure S2).
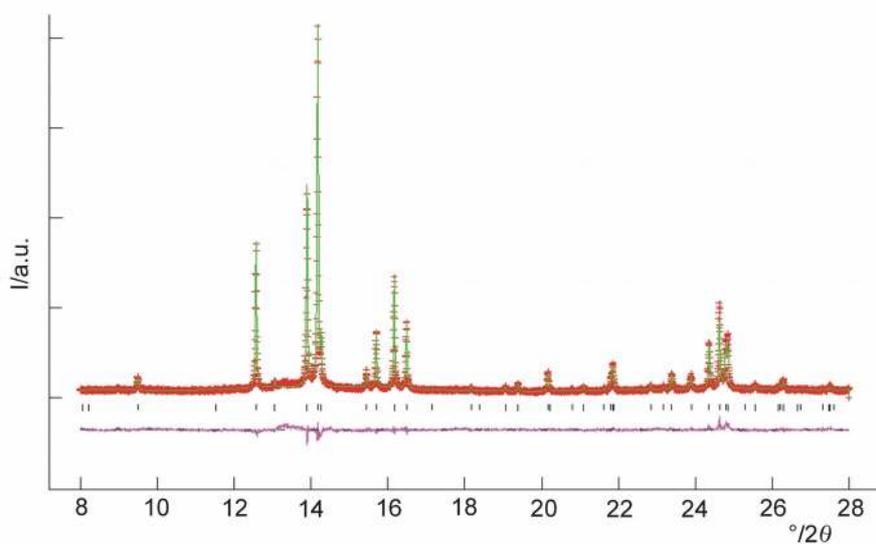
Figure 2 Synchrotron powder data after Rietveld refinement of the structure of Ni_7B_3 with a Th_7Fe_3-based disordered model (red: observed; green: calculated; purple: difference curve; vertical dashes indicate the positions of the symmetry allowed reflections)

Table 1 Crystallographic data for Ni7B3

Formula	Ni_7B_3
Crystal system	hexagonal
Space group	$P6_3mc$ (no. 186)
Lattice parameters/pm	
a	696.836(4)
c	439.402(4)
$V/Å^3$	184.7800(2)
$\square$/Å	0.499694
T/K	300
Background polynomial, No. of parameters	shifted Chebyschev 10
Zero shift	$\square$0.00242(6)
No. of reflections	90
No. of structure parameters	19
wR_p	0.0885
R_p	0.0669

7

χ^2	2.119
D_{wd}	0.942
$\rho_{max}/e\text{Å}^{-3}$	2.39
$\rho_{min}/e\text{Å}^{-3}$	-2.61

Table 2 Positional and isotropic displacement parameters, site occupancies of Ni_7B_3. The values in brackets refer to standard deviations.

| Atom	Wyckoff site	*x/a*	*y/b*	*z/c*	SOF	U_{iso}
Ni1	2*b*	1/3	2/3	0.803(3)	1	0.01(7)
Ni2	6*c*	0.4585(1)	0.5415(1)	0.302(2)	1	0.01(4)
Ni3	6*c*	0.1222(3)	0.8778(3)	0.6013(6)	0.52(1)	0.009(5)
Ni4	6*c*	0.1245(3)	0.8755(3)	0.0253(6)	0.48(1)	0.009(5)
B6	6*c*	0.812(2)	0.188(5)	0.480(7)	0.48(5)	0.025(4)
B7	6*c*	0.201(2)	0.799(2)	0.550(6)	0.52(5)	0.025(4)

Usually, the Th_7Fe_3-structure type manifests itself in metal borides M_7B_3 (Ru, Rh, Tc) like this: the metal atoms occupy three sites (2*b*, 2 x 6*c*) and the boron atom is located at an additional 6*c* site. *Fokwa* et al.[31] described the crystal structure by boron-centered trigonal prisms of metal atoms, of which three share one corner (metal atom at 2*b*). Such entities are connected to each other forming a three-dimensional network. Also, there are empty, face-sharing octahedra M_6 that form one-dimensional columns along [001].

In Ni_7B_3, nickel atoms Ni3 and Ni4 form columns of face-sharing octahedra of two orientations, penetrating each other. Rotation of a column of octahedra around 180° transforms it into the other one. The superposition of the two half-occupied columns is shown in figure 3.
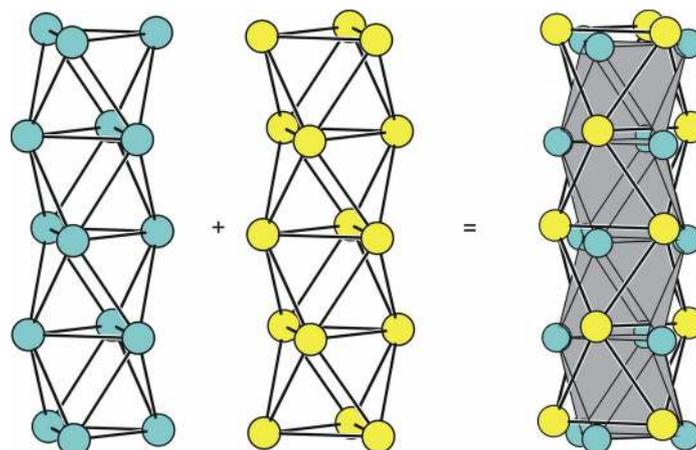
Figure 3 Representation of the two columns of face-sharing Ni_6 octahedra and their superposition in the disordered model of Ni_7B_3

This split model results of course in two additional boron sites and thus in two types of boron-centered trigonal prisms: Ni1, Ni2, and Ni3 coordinate B6, and Ni1, Ni2, and Ni4 coordinate B7. The two types of prisms are penetrating each other as shown in figure 4. Figure 5 shows the unit cell of nickel boride, Ni_7B_3, in direction of the *c* axis.
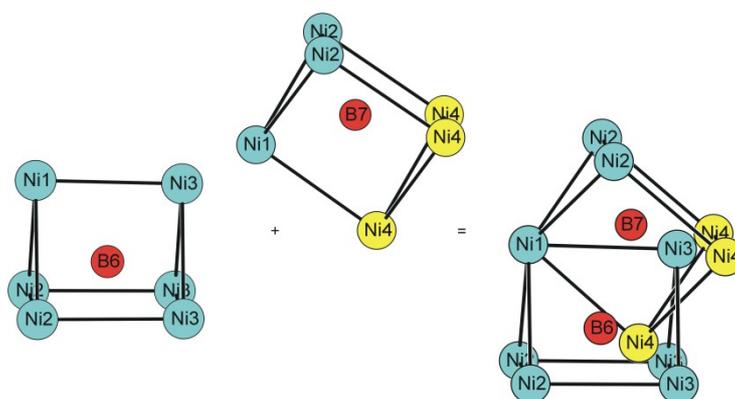

Figure 4 Two boron-centered prisms of nickel atoms and the resulting disordered model (red: boron atoms; blue/yellow: nickel atoms)
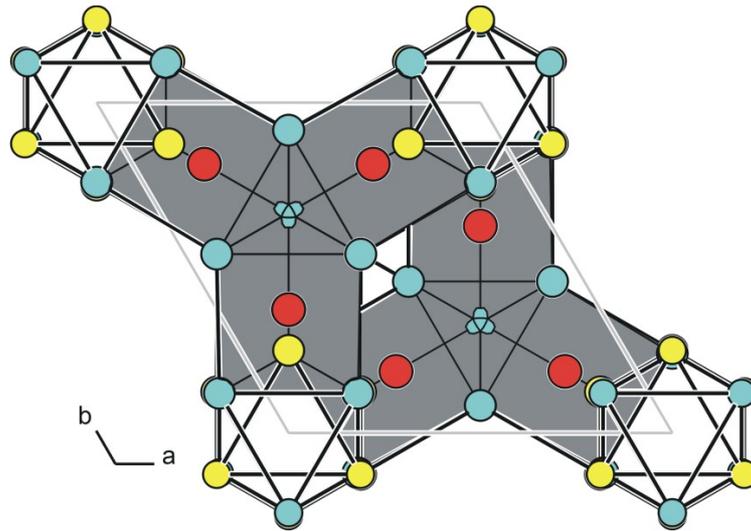
Figure 5 Unit cell of Ni_7B_3. View along [001] (red: boron atoms; blue/yellow: nickel atoms)

Magnetic properties, observed and calculated. As shown in figure 6, metal-rich Ni_7B_3 was found to be paramagnetic. A small ferromagnetic impurity was detected that is invisible in X-ray diffraction. This was seen in the slight hysteresis at room temperature. It was attributed to elemental nickel. By comparing the measured saturation magnetization with that expected for nickel metal (≈ 0.6 µB/Ni), the estimated nickel impurity is less than 0.5 wt%.
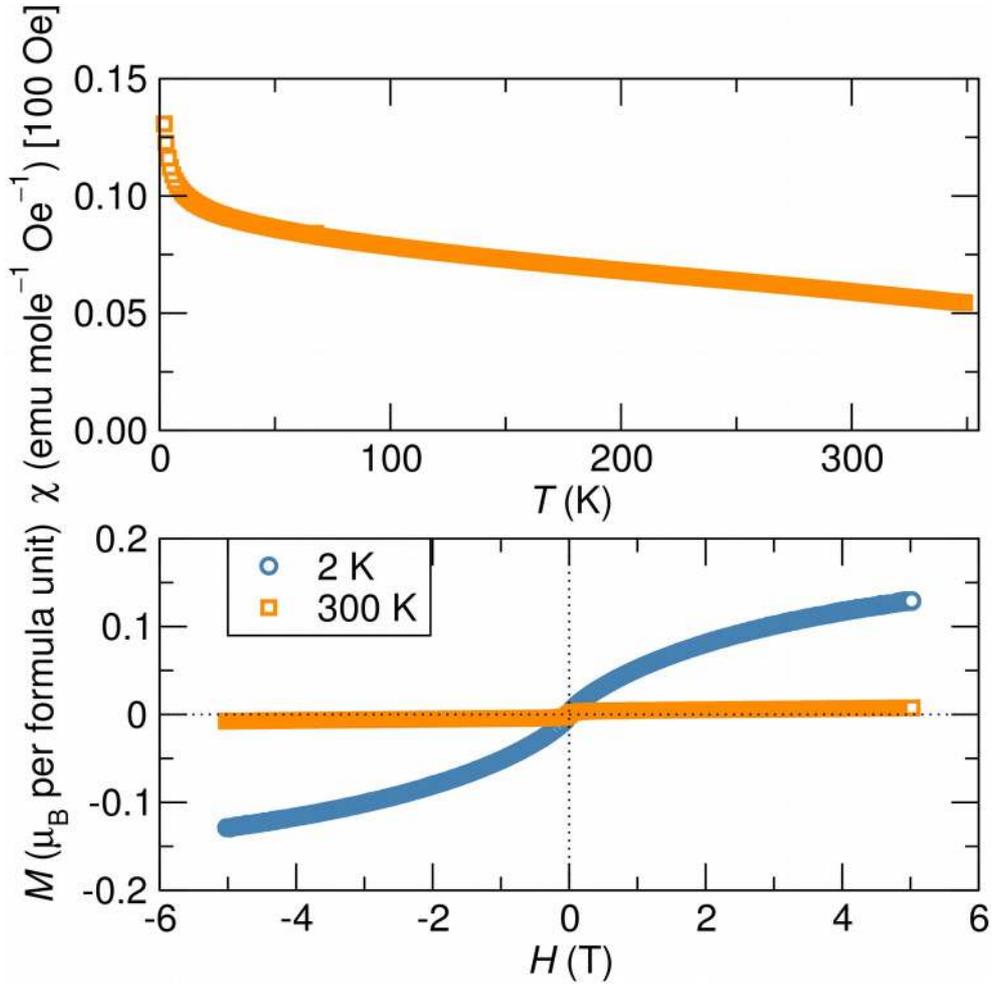
Figure 6 Magnitization of Ni_7B_3 at room temperature and 2 K (bottom); field-cooled susceptibility measurement (top)

The experimental crystal structure data of Ni_7B_3 was idealized to the ordered Th_7Fe_3-structure type and taken as starting point for the DFT calculations. Structure optimization was performed and the energy-volume relationship of the Ni_7B_3 structure was calculated at different volumes and the results were fitted to the third-order Birch-Murnaghan equation of state.[43] The calculated lattice constants as well as the equilibrium volume (a = 698 pm, c = 438 pm, V = 184.63 Å^3) are in good agreement with experimental measurements. The total density of states (Fig. 7) is consistent with the absence of magnetic ordering, since there is no spin splitting between spin components and the population of spin up and spin down states are the same.
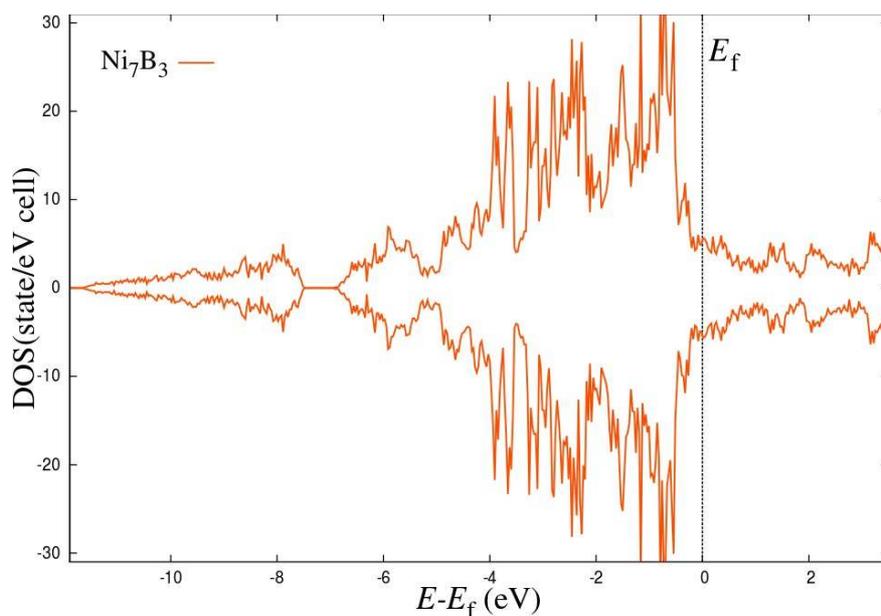
Figure 7 Total density of state for Ni_7B_3, spin up with positive values, spin down with negative values. Dashed line represents the Fermi level (E_F).

High-temperature stability. Differential scanning calorimetry was run up to 800 °C and displayed an exothermic effect at 424 °C (Fig. 8). Afterwards, the XRD pattern of the sample exhibited the reflections of Ni_3B and Ni_2B. The high-temperature XRD measurement (Fig. 9, see also Supporting Information, Figure S3) revealed that Ni_7B_3 starts to crystallize at 350 °C. Around 370 °C all of the reflections of Ni_7B_3 are present, plus some small reflections that are indicative of the presence of Ni_3B. Starting at 380 °C, the formation of Ni_2B can be detected. The intensity of the Ni_7B_3 reflections decreases significantly at about 460 °C and vanishes at 760 °C. Above this temperature only Ni_3B and Ni_2B can be detected with increasing crystallinity.
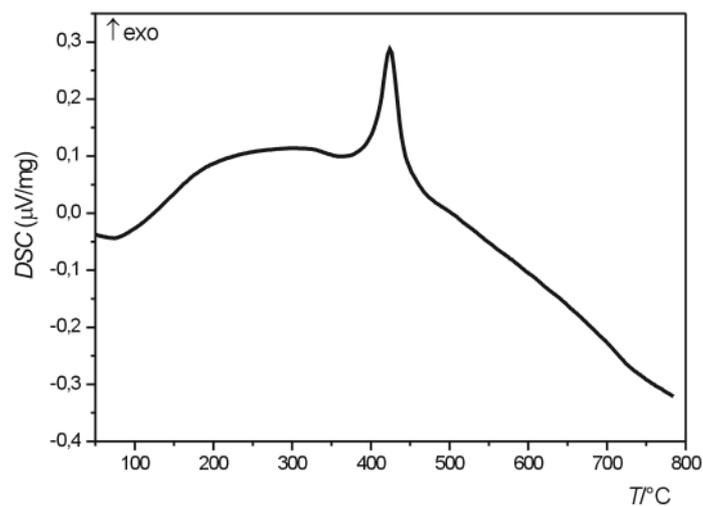
Figure 8 DSC measurement of Ni$_7$B$_3$
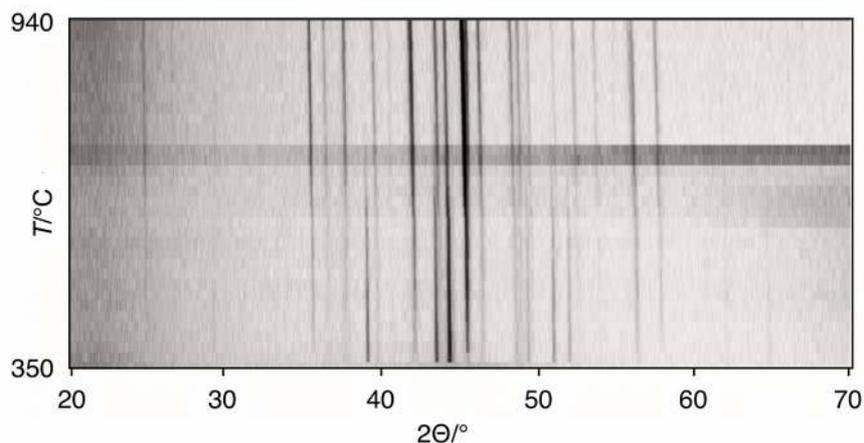
Fig. 9 High temperature-XRD measurements of Ni$_7$B$_3$

Conclusions

The Ni-B system was found to contain a metastable, metal-rich phase, Ni$_7$B$_3$, that is not ferromagnetic and crystallizes in a formerly unknown disordered variant of the Th$_7$Fe$_3$-structure type, as determined from synchrotron powder data. Its stability temperature range is very narrow according to high temperature XRD and DSC measurements. Magnetic measurements and quantum chemical calculations are in accordance.

Supporting information available: SEM image to show nanostructure; alternate presentation of Fig. 9; refinement results for X-ray data collected with CuK$_{\alpha1}$ radiation.

Acknowledgements

References

(1) Albert, B., Hillebrecht, H. *Angew. Chem. Int. Ed.* **2009**,*48*, 8640–8668.

(2) Fokwa, B. P. T. *Encyclopedia of Inorganic and Bioinorganic Chemistry* **2014**, 1–14.

(3) Kapfenberger, C., Hofmann, K., Albert, B. *Solid State Sci.* **2003**, *5*, 925–930.

(4) Rades, S., Kornowski, A., Weller, H., Albert, B. *ChemPhysChem* **2011**, *12*, 1756–1760.

(5) Rades. S. Kraemer, S. Seshadri, R. Albert, B. *Chem. Mater.* **2014**, 1549-1552

(6) Ploss, M. Facey, S. J., Bruhn, C., Zemel, L., Hofmann, K., Stark, R. W., Albert, B., Hauer, B. BMC Biotechnology **2014**, *14*, 12.

(7) Caputo, R., Guzzetta, F., Angerhofer, A. *Inorg. Chem.* **2010**, *49*, 8756-8762.

(8) Portehault, D., Devi, S., Beaunier, P., Gervais, C., Giordano, C., Sanchez, C., Antonietti, M. *Angew. Chem. Int. Ed.* **2011**, *50*, 3262□3265.

(9) Carenco, S., Portehault, D., Boussière, C., Mézailles, N., Sanchez, C. *Chem. Rev.* **2013**, *113*, 78981□8065.

(10) Bykova, E., Tsirlin, A. A., Gou, H., Dubrovinsky, L., Dubrovinskaia, N. *J. Alloys Comp.* **2014**, *608*, 69□72.

(11) Xie, Z., Graule, M., Orlovskaya, N., Payzant, E. A., Cullen, D. A., Blair, R. G. *J. Solid State Chem.* **2014**, *215*, 16□21.

(12) Xie, Z., Blair, R. C., Orlovskaya, N., Cullen, D. A., Payzant, E. A. *J. Solid State Chem.* **2014**, *219*, 210□219.

(13) Xie, Z., Lugovy, M., Orlovskaya, N., Graule, T., Kübler, H., Müller, M., Gao, H., Radovic, M. Cullen, D. A., *J. Alloys Comp.* **2015**, *634*, 168-178.

(14) Cumberland, R. W., Weinberger, M. B., Gilman, J. J., Clark, S. M. Tolbert, S. H., Kaner, R. B., *J. Amer. Chem. Soc.* **2005**, *127*, 7264-7265.

(15) Chung, H. Y., Weinberger, M. B., Levine, J. B., Kavner, A., Yang, J.-M., Tolbert, S. H., Kaner, R. B. *Science*, **2007**, *316*, 436□439.

(16) B. Idzikowski, A. Szajek, *J. Optoelec. Adv. Mater.* **2003**, *5*, 293 – 244.

(17) Rundquist, S. *Acta Chem. Scand.* **1958**, *12*, 658 – 662.

(18) Monnier, G., Rieviere, R., Ayel, M. *Compt. Rend.* **1967**, *C24*, 862 – 865.

(19) Rundquist, S. *Am. Ceram. Soc.* **1959**, *13*, 1193 – 1208.

(20) Blum, P. *J. de Physique et du Radium*, **1952**, *1*, 430 – 431.

(21) Lundström, T., Tergenius, L. E., Higashi, I. *Z. Kristallogr.* **1984**, *167*, 235 – 246.

(22) Bratkovsky, A. M., Rashkeev, S. N., Wendin, G. *Phys. Rev.* **1993**, *B48*, 6260□6270.

(23) Schaefer , Z. L., Ke, X., Schiffer, P., Schaak, R. E., *J. Phys. Chem. C* **2008**, 19846□19851.

(24) Wodniecka, B. Wodnieki, P., Królas, K., Thomé, L. *J. Phys. F: Met. Phys.* **1986**, *16*, 1629 – 1637.

(25) Kher, S. S., Spencer, J. T. *Chem. Mater.* **1992**, *4*, 538 – 544.

(26) Punge-Witteler, B., Köster, U. *Mat. Sci. Eng.* **1988**, *97*, 343 – 346.

(27) Machizaud, F., Kuhnast, F.-A., Flechon, J., Auguin, B., Defresne, A. *J. Physique* **1981**, *42* (1981) 97 – 106.

(28) Aronson, B. *Acta. Chem. Scand.* **1959**, *13*, 109 – 114.

(29) Stenberg, E., Aselius, J. *Acta Chem. Scand.* **1960**, *14*, 733 – 741.

(30) Trzebiatowski, W. Rudzinski, J. *J. Less Comm. Metals* **1964**, *6*, 244 – 245.

(31) Misse, P. R. N., Dronskowski, R., Fokwa, B. P. T. *Z. Naturforsch.* **2011**, *66b*, 1241 – 1247.

(32) a) Toby, B. H. EXPGUI, a graphical user interface for GSAS, *J. Appl. Cryst.* **2001**, *34*, 210 – 21; b) Larson, A. C., Von Dreele, R. B. "General Structure Analysis System (GSAS)" Los Alamos National Laboratory Report LAUR **2004**, 86 – 748.

(33) Further details of the crystal structure investigation may be obtained from Fachinformationszentrum Karlsruhe, 76344 Eggenstein-Leopoldshafen, Germany (fax: (+49)7247-808-666; e-mail: crysdata@fiz-karlsruhe.de, http://www.fiz-karlsruhe.de/request_for_deposited_data.html) on quoting the CSD number 430071.

(34) Hohenberg, P., Kohn, W. *Phys. Rev. B* **1964**, *136*, 864.

(35) Blöchl, P. E. *Phys. Rev. B* **1994**, *50*, 17953.

(36) Kresse, G., Furthmüller, J. *Phys. Rev. B* **1996**, *54*, 11169.

(37) Perdew, J. P., Burke, K., Ernzerhof, M. *Phys. Rev. Lett.* **1996**, *77*, 3865.

(38) Methfessel, M., Paxton, A. T. *Phys. Rev. B* **1989**, *40*, 3616.

(39) Monkhorst, H. J., Pack, J. D. *Phys. Rev. B* **1976**, *13*, 5188.

(40) Bylander, D. M., Kleinman, L., Lee, S. *Phys Rev. B.* **1990**, *42*, 1394.

(41) Brown, H. C., Brown, C. A. *J. Am. Chem. Soc.*, **1962**, *84*, 14931494.

(42) Kapfenberger, C. Synthese und Charakterisierung von nano-skaligen Nickelboriden, *PhD Thesis* **2005**, Universität Hamburg.

(43) Brich, F. *Phys. Rev.* **1947**, *71*, 809–824.

For table contents only
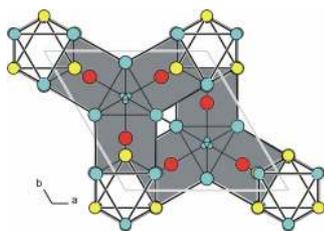
A new, metastable nickel boride, Ni_7B_3, is trapped by applying low-temperature solution synthesis. Its crystal structure is an unknown, disordered variant of the Th_7Fe_3-structure type, solved from synchrotron X-ray powder data. Magnetic measurements reveal paramagnetism, which is in accordance with quantum chemical calculations. According to high-temperature X-ray diffraction and differential scanning calorimetry this nickel boride phase has a narrow stability window.

Metastable Ni₇B₃: A New Paramagnetic Boride from Solution chemistry, Its Crystal structure and Magnetic properties

Kathrin Hofmann,[a] Nalan Kalyon,[a] Christine Kapfenberger,[a] Leo Lamontagne,[b] Salman Zarrini,[c] Robert Berger,[c*] Ram Seshadri,[b*] and Barbara Albert[a*]

[a] Eduard-Zintl-Institute of Inorganic and Physical Chemistry, Technische Universität Darmstadt, Alarich-Weiss-Str. 12, 64287 Darmstadt, Germany

[b] Materials Department and Materials Research Laboratory, University of California Santa Barbara, Santa Barbara CA 93106, U.S.A.

[c] Fachbereich Chemie, Philipps-Universität Marburg, Hans-Meerwein-Str. 4, 35032 Marburg, Germany

*corresponding author: albert@ac.chemie.tu-darmstadt.de (B. Albert), Tel. +49-(0)6151-162392, FAX +49-(0)6151-166029

Supporting Information submitted to Inorg. Chem.
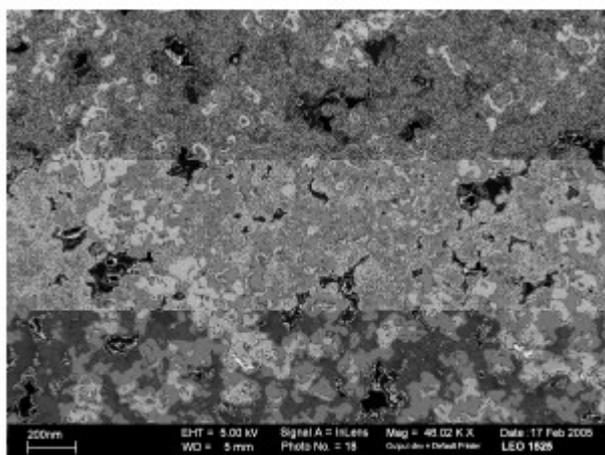
Fig. S1 Scanning electron micrograph, Zeiss Leo 1525- SEM

Fig. S2 Rietveld fit of powder pattern collected with Cu Kα_1 radiation, wR$_p$: 0.0611; R$_p$; 0.0462, D$_{wd}$: 0.940; χ^2: 1.692
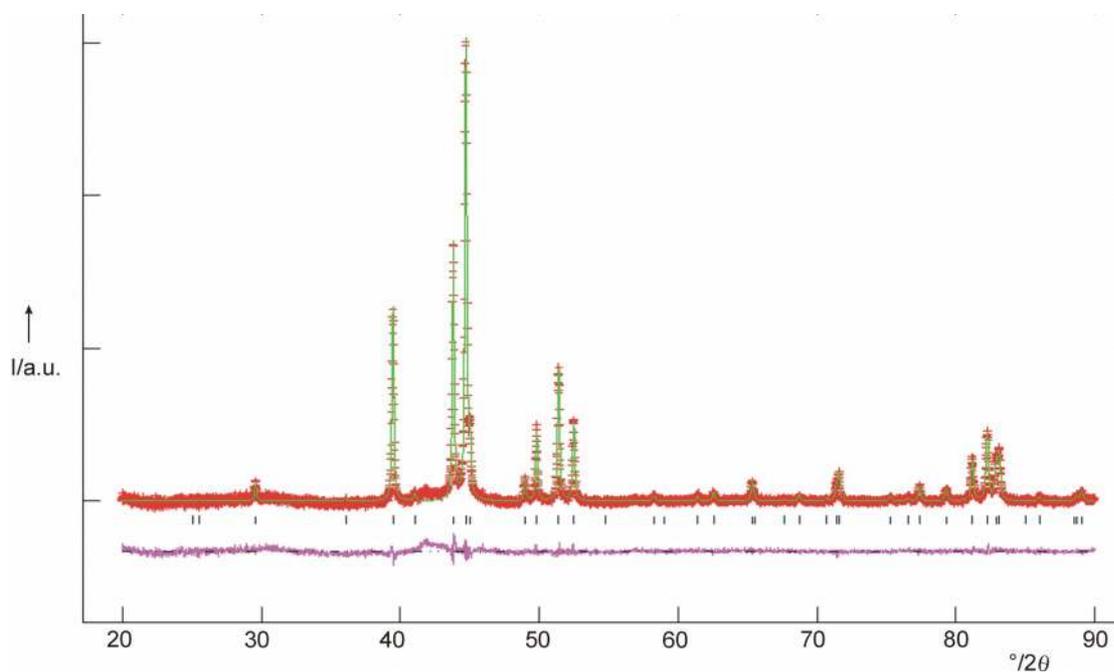
Table S1: Atomic parameters and isotropic thermal displacement parameters (Rietveld refinement based on lab data measured with Cu Kα_1 radiation)

Atom	Wyckoff-site	x/a	y/b	z/c	occ	Uiso
Ni1	2b	1/3	2/3	0.806(2)	1	0.0229(9)
Ni2	6c	0.4582(1)	0.5418(1)	0.302(3)	1	0.0248(5)
Ni3	6c	0.1216(3)	0.8784(3)	0.6018(6)	0.52	0.0222(6)
Ni4	6c	0.1239(3)	0.8761(3)	0.0251(7)	0.48	0.0222(6)
B6	6c	0.806(2)	0.194(2)	0.455(6)	0.48	0.030(4)
B7	6c	0.204(2)	0.796(2)	0.559(6)	0.52	0.030(4)

Fig S3. *ht*-X-ray diffraction patterns (different type of presentation of the same data as shown in Fig. 9)